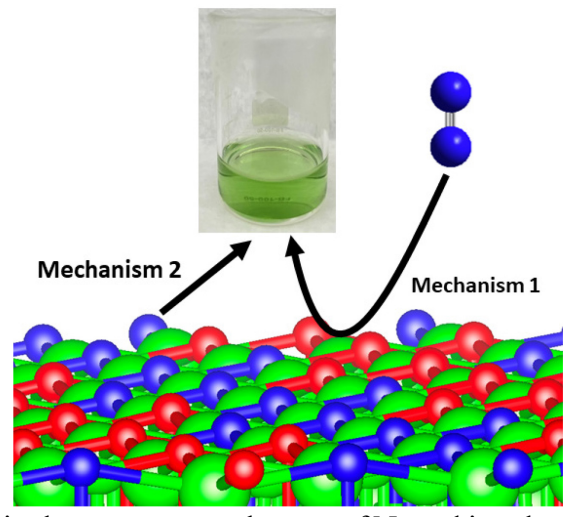
Electro-catalytic Reduction of Nitrogen to Ammonia: The Roles of Lattice O and N in Reduction at Vanadium Oxynitride Surfaces

Adaeze Osonkie,[†] Ashwin Ganesan,[†] Precious Chukwunenye, Fatima Anwar, Kabirat Balogun, Mojgan Gharee, Ishika Rashed, Thomas R. Cundari, * Francis D'Souza* and Jeffry A. Kelber* Department of Chemistry, University of North Texas, 1155 Union Circle, #305070, Denton, TX 76203-5017, USA

KEYWORDS: Electrocatalysis, X-ray photoemission spectroscopy, nitrogen reduction reaction, Density functional theory, vanadium oxynitride

ABSTRACT: Vanadium oxynitride and other Earth-abundant oxynitrides are of growing interest for the electrocatalytic reduction of nitrogen to NH₃. A major unresolved issue, however, concerns the roles of lattice N and lattice O in this process. Electrochemistry and photoemission data reported here demonstrate that both lattice N and dissolved N₂ are reduced to NH₃ by cathodic polarization of vanadium oxynitride films at pH 7. These data also



show that ammonia production from lattice N occurs in the presence or absence of N_2 and involves the formation of $V\equiv N$: intermediates or similar unsaturated VN surface states on a thin vanadium oxide overlayer. In contrast, N_2 reduction proceeds in the presence or absence of lattice N, and without N incorporation into a vanadium oxide lattice. Thus, both lattice N and N_2 reduction mechanisms involve oxide-supported V surface sites ([V]_O) in preference to N-supported sites ([V]_N). This result is supported by DFT-based calculations showing that the formation of V \equiv N:, V-N=N-H, and a few other plausible reaction intermediates are consistently energetically favored

[‡]Equal contribution

at [V]o rather than at [V]_N surface sites. Similar effects are predicted for the oxynitrides of other oxophilic metals, such as Ti.

INTRODUCTION

The reduction of N₂ to NH₃ is vital to agriculture and mainly accomplished by the Haber-Bosch process, which currently accounts for ~2% of global energy consumption.¹ The Haber-Bosch process also produces CO₂ due to the use of fossil fuels to run the reaction at elevated temperatures.¹ Electrocatalytic reduction of N₂—the nitrogen reduction reaction (NRR)—is a plausible, environmentally-friendly alternative route to NH₃ production.¹ A variety of electrocatalysts, including noble and non-noble metals, metal oxides (doped and un-doped), and metal nitrides, have been the subjects of recent investigations.²⁻⁷ A broad range of Faradaic Efficiencies (FEs) have also been reported, varying with both materials and reaction conditions.^{1,8} A particular problem complicating such investigations is the competitive hydrogen evolution reaction (HER), which reduces NH₃ yields and kinetics, and has prompted the investigation of metal-free catalysts.^{9,10}

Metal oxynitrides and nitrides have received significant attention as NRR catalysts, and are generally thought—particularly based on N isotope exchange studies—to exhibit a Mars-Van Krevelen (MVK) type reaction mechanism, in which lattice N is reacted to form NH₃, and subsequently replaced by N₂ from solution.^{7,11-13} The presence or absence of a general MVK mechanism is obviously of considerable practical relevance in understanding the use, durability and/or depletion of N in oxides and oxynitrides. A directly related issue is the role of nitrogenmetal vs oxygen-metal interactions in N₂ binding and subsequent protonation. Understanding such issues in detail can assist with the design of catalysts that are both efficient in binding N₂ and relatively selective in NRR vs. HER.

Herein, we focus on vanadium oxynitrides^{12,13} and vanadium oxides,¹⁴ which have been the subjects of recent NRR investigations. Electrochemical and ion-exchange studies under acidic conditions^{12,13} have established that for VN nanoparticles, vanadium-oxynitride is the NRR-active phase, with pure VN being inactive.¹² These findings were corroborated by recent studies¹⁴ reporting that N-free V(III)/V(IV) oxides are NRR-active in neutral electrolytes. DFT-based calculations¹⁴ also indicated that the dissociation of bound N_2 at vanadium sites ([V]):

$$[V]-N_2 \rightarrow [V] \equiv N: + \frac{1}{2} N_2 \tag{1}$$

is energetically favored by almost 18 kcal mole⁻¹ at O-ligated V centers relative to N-ligated V centers. A similar trend was observed in calculations for other oxophilic transition metal sites.¹⁴ Other theoretical studies,¹⁵ however, have focused on the protonation of surface N sites, concluding that a relatively low O content (12.5%) in the oxynitride phase optimizes the protonation of N surface sites over V sites. The issues to be elucidated, therefore, concern the roles of lattice O and lattice N in (a) the initial binding and subsequent reaction of N₂ at the oxynitride surface; and (b) the extent to which the binding and reaction of N₂ results in incorporation of N in the lattice (the MVK mechanism), or whether the reactions of N₂ and surface lattice N are distinct from each other.

In probing gas/surface interactions, surface-sensitive probes such as X-ray photoelectron spectroscopy (XPS) have been, for some time, a critical tool for understanding heterogeneous catalysis reaction mechanisms, and for optimizing catalyst activity and selectivity. Corresponding studies at the electrolyte/solid interface are, however, a still-developing area of research. He-22 With respect to vanadium oxynitrides, recent ex situ photoemission studies on vanadium nitride nanoparticles have shown that vanadium oxynitrides formed in situ are the active species and that an N surface state with an N 1s binding energy of 396.5 eV is associated with NRR activity. Moreover, the relative photoemission intensity of that feature correlated with the NRR activity of the nanoparticle. Recent experimental and theoretical studies have identified this N 1s binding energy at 396.5 eV is consistent with the transformation of lattice N to V≡N: or similar unsaturated VN surface configuration—which are plausible NRR intermediates 1.13—on top of a thin vanadium oxide overlayer.

The investigation of such surface transformations at the electrolyte/surface interface by use of ex situ XPS or similar methods must of course exercise due caution given possible effects of ambient exposure. Such a transformation of the vanadium oxynitride cannot, however, be produced by exposure to O₂ or H₂O.^{23,24} As shown below, such a transformation of lattice N and the oxynitride surface is, however, also observed by ex situ XPS after cathodic polarization of the V oxynitride surface in neutral electrolyte. The inability to produce such surface transformation upon oxidation by O₂ or H₂O indicates that such transformation cannot be ascribed to ambient

exposure. As such, in this particular instance, the cautious use of ex situ XPS as a surface probe is justified.

In this report, ex situ XPS and theoretical studies are coupled with electrochemical measurements on vanadium oxynitride surfaces of varying N/O ratios, and on vanadium oxide surfaces. In order to identify the possible distinctions in ammonia production reactions of adsorbed N₂ vs lattice N, studies are carried out in both N₂-saturated and Ar-saturated solvents and compared to results on blank fluorinated tin oxide (FTO) substrates. In contrast to previous oxynitride studies, ^{12,13} but consistent with our previously-reported studies on vanadium oxide, ¹⁴ electrochemical studies were carried out at pH 7, in order to minimize the possible role of the hydrogen evolution reaction (HER).

Herein, we demonstrate that the N 1s feature at 396.5 eV binding energy is also produced by cathodic polarization of a vanadium oxynitride surface, in the presence or absence of dissolved N₂, coincident with the formation of a thin, V(III)/V(IV) mixed oxide surface layer, in pH 7 solution, with the corresponding production of NH₃. As previously reported, electrochemical measurements also demonstrate that NH₃ production from dissolved N₂ occurs at an N-vacant vanadium oxide surface. He is situ photoemission indicates that this occurs without the apparent incorporation of N into the oxide lattice. Thus, experiments indicate that reduction of lattice N to NH₃ in vanadium oxynitrides occurs via formation of V=N: or similar reaction intermediate formed on top of a vanadium oxide surface layer, independent of the presence of dissolved N₂. In contrast, dissolved N₂ reduction to NH₃ occurs at a vanadium oxide surface devoid of lattice N, and without incorporation of N into the lattice. These results are corroborated by DFT-based calculations showing that the formation of V=N: and various other plausible reaction intermediates (e.g., V-NNH) are consistently energetically favored at [V]o rather than at [V]_N Lewis acid sites.

METHODS

Theory

All computations were performed using the Vienna ab initio simulation package (version 5.4.4). Sall simulations were spin polarized and implemented generalized gradient approximation and projector-augmented wave methods. Calculations utilized an energy cutoff of 500 eV, while SCF convergence was < 1 x 10-5 eV. Surface calculations were done in a unit cell of 8.09 x 8.09 x 28.79 Å, a K-point mesh²⁶ of 3 x 3 x 1, and the Methfessel-Paxton method²⁷ with $\sigma = 0.2$ eV. The models studied were rock salt VN(100) surfaces, with various adatoms ligated to a Lewis acidic V center, as validated in previous studies. Calculations suggest that the (100) surface is more stable than the (111) surface for VO_xN_y. Moreover, recent work by Sangiovanni *et al.* and Gudmundsson *et al.* indicates that the (100) surface for vanadium nitride – our VO_xN_y model is relatively N-rich – is more catalytically active. For these reasons, modeling efforts focused on the (100) surface. Also, the (111) surface is polar and therefore undergoes extensive reconstruction akin to what has been discussed by Cappus *et al.* for metal oxides. Hence, although the (111) surface may be prevalent, it may not be the most catalytically active surface. The (100) surface is exposed to ~20 Å of vacuum.

Experiment

Oxynitride Film Deposition and Analysis: Vanadium oxynitride films (VO_xN_{1-x}; 0 < x < 1) for electrochemical analysis were deposited in a turbo molecularly-pumped magnetron sputter deposition system, with a commercial magnetron source (Meivac, Inc.), described previously. Films were deposited on commercially available fluorinated tin oxide (FTO) substrates. The base pressure of this system was 5 x 10^{-8} Torr.

Prior to film deposition, the substrates were annealed in oxygen at 10⁻⁶ Torr to 900 K for 3 hours to remove adventitious C and other contaminants. Magnetron sputter deposition was done using a 99.9% purity V target at 673 K, and a combination of electronic grade N₂ and O₂ gases, at total pressures of 4 mTorr, 25 W power for 7 mins. Although film thicknesses were not measured directly, previous experiments under very similar conditions consistently yielded films ~500 Å thick. 14,23,28 In situ analyses of V/O/N atomic ratios were carried out using a commercial Auger single pass cylindrical mirror analyzer with a concentric electron gun. Auger spectra were acquired at 3 KeV electron beam energy.

After Auger spectroscopy, several films were selected for further characterization by optical microscopy and AFM. Both optical and atomic force microscopy studies were carried out at the UNT Materials Research Facility using a Nikon Eclipse ME600 Digital Optical Microscope, and a VEECO Multimode Nanoscope III AFM tapping mode with a tip force constant of 40 N/m. Other films were subjected to EC polarization (see below), emmersed at controlled potential, rinsed, and then characterized by optical and AFM microscopies.

X-ray diffraction (XRD) 2θ scans were also acquired for several films using a Rigaku Ultima III Instrument employing Cu K α radiation ($\lambda = 1.541$ Å).

After deposition, most films were transferred in ambient to a second vacuum system for XPS analysis. This system has been described previously.³² Briefly, this system consisted of an XPS analysis chamber, and an attached chamber containing a custom built, inductively coupled plasma source. XPS spectra were acquired in constant pass energy mode (23.5 eV) using a commercial hemispherical analyzer (Physical Electronics) with a microchannel plate detector, and Al Kα radiation from an unmonochromatized source operated at 300 W, 15 KeV. Analysis of XPS data was carried out by standard methods.³³ Peak fitting employed Gaussian-Lorentzian components and was carried out as described previously.²³ In general, O/N atomic ratios derived from in-situ Auger analysis agreed well with those obtained from ex situ XPS. However, the results from XPS analysis are used here, as all films underwent exposure to ambient prior to both XPS analysis and to electrochemical testing. XPS binding energies were calibrated by setting the V 2p_{3/2} VN component binding energy at 513.5 eV.^{23,24}

After XPS, the sample was transferred to ambient for electrochemical studies. Electrochemical measurements were carried out in a three-electrode electrochemical cell in a 0.1 M Na₂SO₄ (pH = 7) electrolyte saturated with either Ar or N₂, using an EG&G 263A potentiostat/galvanostat. An Ag/AgCl reference electrode and platinum wire counter electrode were used. Linear sweep voltammograms were recorded on the reductive side for the vanadium oxide films deposited onto FTO glass substrates. Control studies were also performed on plain conductive FTO glass as the working electrode. Multi-cyclic voltammograms (15 cycles) were recorded under the same electrochemical conditions to evaluate the robustness of the catalyst films.

In order to eliminate trace amounts of ammonia and/or NO₂/NO₃ impurities present in the nitrogen gas, N₂ was passed through two traps one containing 0.1 M HCl and the second one 0.1 M KOH during electrochemical polarization and bulk-electrolysis studies.

For product analysis, a 1 cm² vanadium oxynitride or vanadium oxide coated FTO electrode was dipped in 20 mL of 0.1 M Na₂SO₄ under N₂ atmosphere. Electrolysis was performed at an applied potential of -0.70 V vs. Ag/AgCl for 1.5 hours. Next, a 10 mL sample of the electrolyte was treated with 0.5 mL of 0.55 M NaOH containing 5 wt % salicylic acid and sodium citrate, 100 μL of sodium nitroprusside dehydrate, and 100 μL of sodium hypochlorite to generate indophenol blue from the ammonia formed during the bulk hydrolysis experiment. ¹⁴ After maintaining the solution at room temperature for 30 min, the absorbance of the solution was measured using a JASCO V-670 spectrophotometer. A control experiment using commercial ammonia to produce indophenol blue using the above procedure was also performed. In both cases, produced indophenol blue revealed similar spectral characteristics.

RESULTS

Structural Characterization

A 2θ XRD scan for a VO_{0.3}N_{0.7} film deposited on FTO is shown in Figure 1. The data show prominent FTO-related diffraction peaks, but also VN(111), VN(220), VN(222), and other features. From the FWHM of the VN-related features (β), crystallite sizes (D) were estimated using the Debye-Scherrer formula:

(1)
$$D = 0.9 \lambda [\beta \cos(\theta)]^{-1}$$

From (1), we estimate the average crystallite size at ~ 15 nm. These results are similar to those reported previously for vanadium oxynitride films prepared by similar methods.³⁴

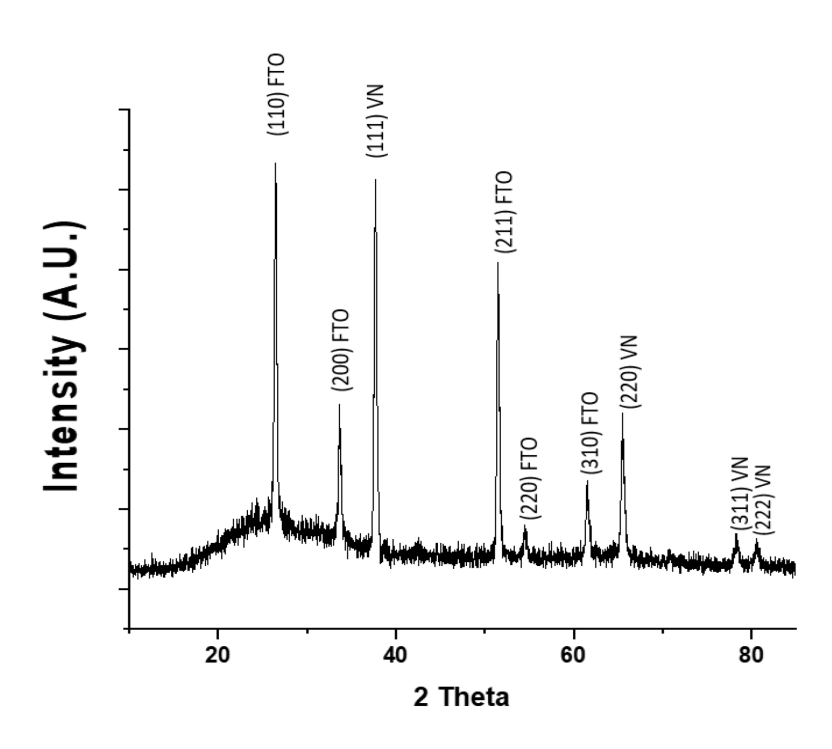


Figure 1. XRD 2θ scan of a VO_{0.3}N_{0.7} film deposited at 400 °C on an FTO substrate.

Typical optical microscopy and AFM measurements acquired on fresh magnetron sputter deposited N-rich vanadium oxynitride films on FTO substrates are shown in Figure 2. The stoichiometry of the film shown in Figure 2 was determined by in situ Auger Spectroscopy to be VO_{0.2}N_{0.8}. Optical microscopy data (Figure 2a) indicate a uniform surface without pits or other discontinuities visible on this scale. 2D and 3D AFM measurements (Figures 2b, c, respectively) and the corresponding roughness histogram (Figure 2d) indicate an RMS roughness of ~36 nm. Similar results were obtained for measurements over other areas of this film, indicating a spatially uniform surface. These morphology and roughness results are also consistent with those recently reported for ~250 Å thick vanadium oxynitride films deposited under similar conditions.³⁴ However, the data in Figure 2 are also consistent with AFM data of an uncoated FTO substrate (not shown), which indicate a similar morphology to that observed in Figure 2b, c. The results are shown in Figures. 1 and 2, therefore, indicate that the VO_xN_y films used in this study, deposited by magnetron sputter deposition, were polycrystalline rather than amorphous, and exhibited moderate surface roughness conformal with that of the FTO substrate. AFM data of a similar film (with a stoichiometry of VO_{0.3}N_{0.7}, but distinct from that shown in Figure 1) acquired after electrochemical cycling in neutral electrolyte yielded a similar RMS roughness value of 31 nm (Supporting Information, Figure S1), indicating negligible change to surface topography during electrocatalysis.

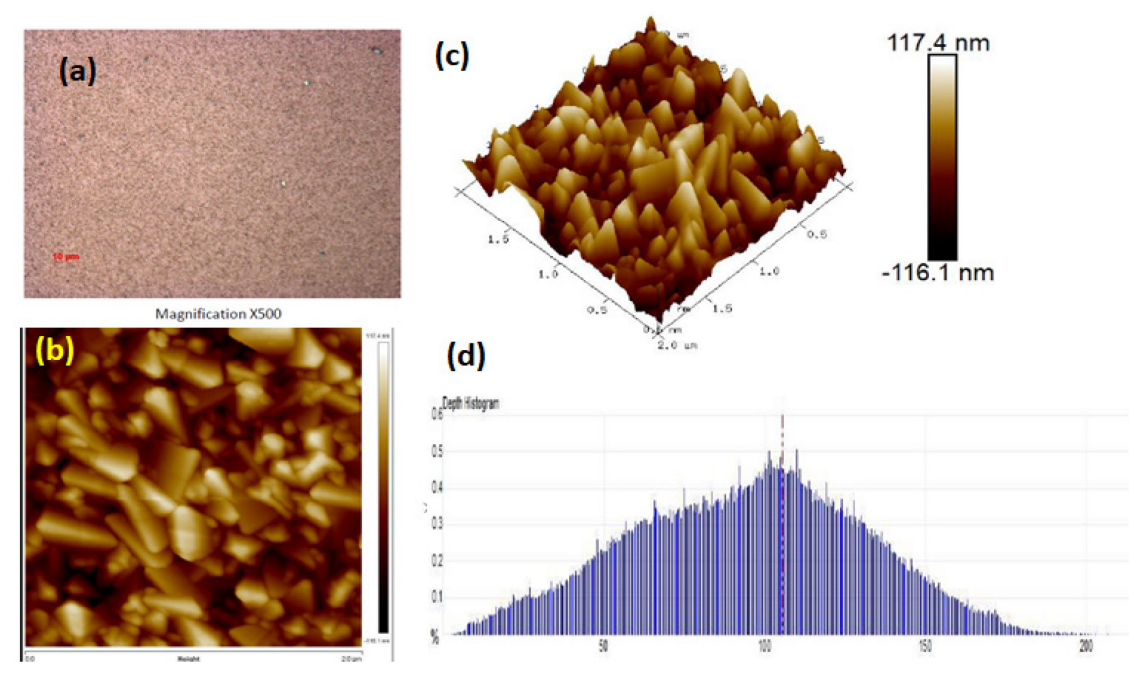


Figure 2. (a) Optical microscopy, (b) 2D AFM and (c) 3D AFM results for a freshly deposited $VO_{0.2}N_{0.8}$ film. (d) Histogram of AFM results, indicating a RMS roughness of 36 nm.

As vanadium oxynitride films are metallic,²³ the electrochemical surface area of V oxynitride films was estimated by cyclic voltammetry using the ferrocene/ferrocenium redox couple and the Randles-Sevcik equation³⁵ (Eqn 2). For such a redox couple, in which diffusion of reactants to/from the surface is the controlling event, the peak scan current (I_p) is linearly proportional to the square root of the scan rate ($v^{1/2}$), expressed in V/sec, according to:

$$I_{p} = 0.4463 \ n \ F \ A \ C \ [n \ F \ v \ D \ / R \ T]^{1/2}$$
 (2)

where n is the number of electrons transferred (n =1), F is the Faraday constant (in C/mol), C is the solution concentration (mol/cm³), and A is the effective electrode surface area (in cm²). Measurements carried out on a film with composition VO_{0.3}N_{0.7} (a different film than in Figure 1) are compared to those for a glassy carbon electrode with a surface area of 0.07 cm². The data (Supporting Information, Figure S2), indicate that the VO_xN_y film has a working electrochemical surface area of 1.82 cm². This is consistent with the overall roughness of the sample (Figure 2) in

comparison to glassy carbon. All films discussed in this work were deposited under very similar conditions, on 1 cm² FTO substrates, and are therefore expected to have similar effective surface areas. In view of the fact that electrochemical polarization induced only minor changes to surface topography (see Figure 2), the working surface area was regarded as stable during electrochemical polarization.

Electrochemical and Photoemission Studies

Cathodic linear polarizations of vanadium oxynitride films with the general composition VO_xN_{1-x} , 0 < x < 1, 23,24 deposited on FTO substrates, were carried out in both Ar-saturated and N_2 -saturated pH 7 solutions. Results are displayed in Figure 3 for a film with x = 0.5. Note that there is relatively little difference in the behavior of the $VO_{0.5}N_{0.5}$ film in Ar-saturated (blue trace, ii) vs. N_2 -saturated solution (red trace, iii). It may be mentioned here that bare FTO (Figure 3, black trace, i) revealed some current in the potential range of -0.2 to -0.7 V, which was also present when the solution was saturated with Ar instead of N_2 . This suggests that the small currents could be due to the reduction of trace amounts of O_2 present in solution or perhaps competing HER activity. Vanadium oxynitride films with varied O/N atomic ratios displayed very similar behavior, however, with slightly higher currents with increased N-content. This is shown in Figure 4, where cathodic linear voltammograms in N_2 -saturated solution are compared for N = 0.5 (red trace, i) and N = 0.7 (dark trace, ii). For the various vanadium oxynitride films tested, similar results were obtained.

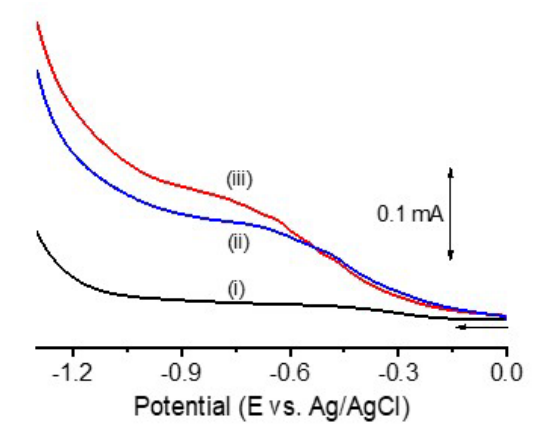


Figure 3. Polarization curves for (i) blank FTO electrode in N₂-saturated solution, (ii) a VO_{0.5}N_{0.5} film on FTO electrode in Ar-saturated Na₂SO₄ solution at pH 7, and (iii) the same VO_{0.5}N_{0.5} film electrode in 0.1 M Na₂SO₄ solution at pH 7 in N₂-saturated solution.

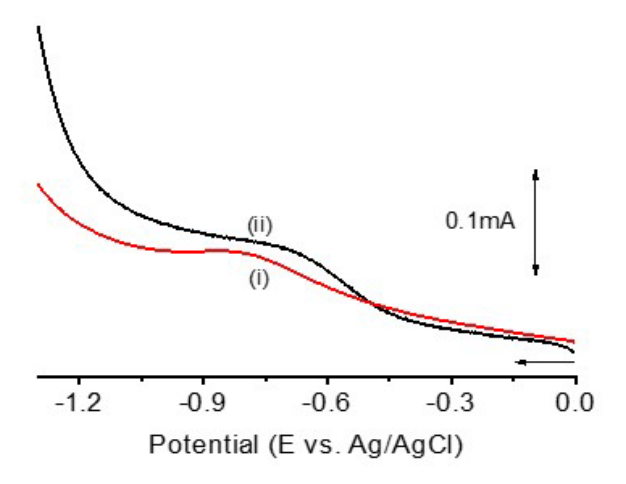


Figure 4. Electrochemical polarization curves for (i) a VO_{0.5}N_{0.5} /FTO film electrode, and (ii) VO_{0.3}N_{0.7}/FTO film electrode in N₂-saturated 0.1 M Na₂SO₄ electrolyte containing solution at pH 7.

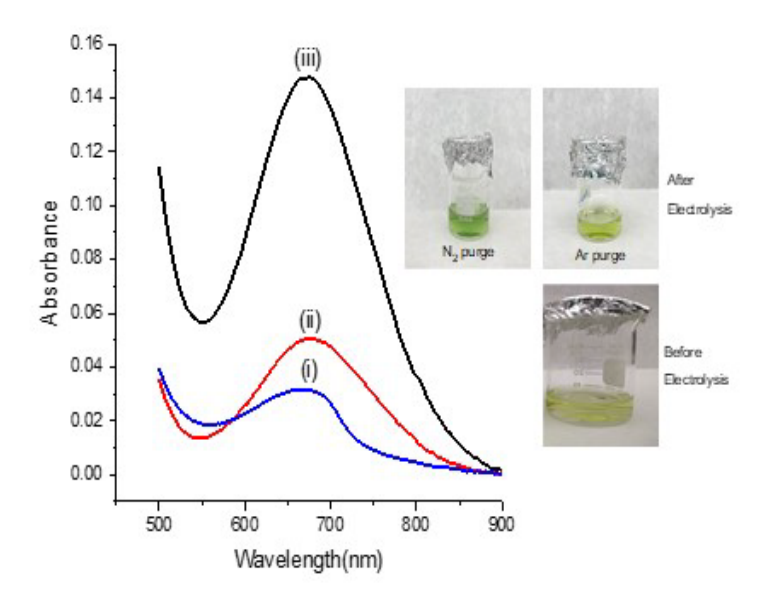


Figure 5. Absorbance spectrum of (i) blank solution prior to electrolysis, (ii) after electrochemical polarization of a VO_{0.7}N_{0.3} film in Ar-saturated solution, (iii) after electrochemical polarization of a VO_{0.7}N_{0.3} film in N₂-saturated solution. Electrolysis was performed in 0.1 M Na₂SO₄ (pH 7). Ar and N purge times were both 10 min. Run time was 90 min at -0.7 eV vs. Ag/AgCl.

Any interpretation of the data in Figures 3 and 4 in terms of NRR activity is of course complicated by the possible coexistence of competing reaction pathways, including HER.¹ However, absorption spectra of indophenol blue¹⁴ confirmed the generation of NH₃ in both Ar-

saturated and N₂-saturated solutions (Figure. 5). These data demonstrate that lattice N can be reduced to NH₃ in the presence or absence of dissolved N₂, consistent with previous isotope-exchange studies on oxynitride nanoparticles.¹³ Notably, the amount of NH₃ produced by a vanadium oxynitride film in the presence of N₂ (Figure 5; black trace, iii), is significantly greater than in Ar-saturated solution (Figure 5; red trace, ii), indicating that the direct reduction of both lattice N and also of N₂ to NH₃ can occur at the same time.

Multi-cyclic voltammetry studies (Figure 6) were also performed on vanadium oxynitride/FTO to check the endurance of the film on the electrode surface. Cycling was performed on a VO_{0.3}N_{0.7} film until no additional changes either in the peak current or position were observed, as shown in Figure 6. During cycling, a small increase in the peak current accompanied by a 20 - 30 mV cathodic shift of the peak potential was observed, suggesting that the film underwent structural changes without significantly losing the deposited material, and more importantly,

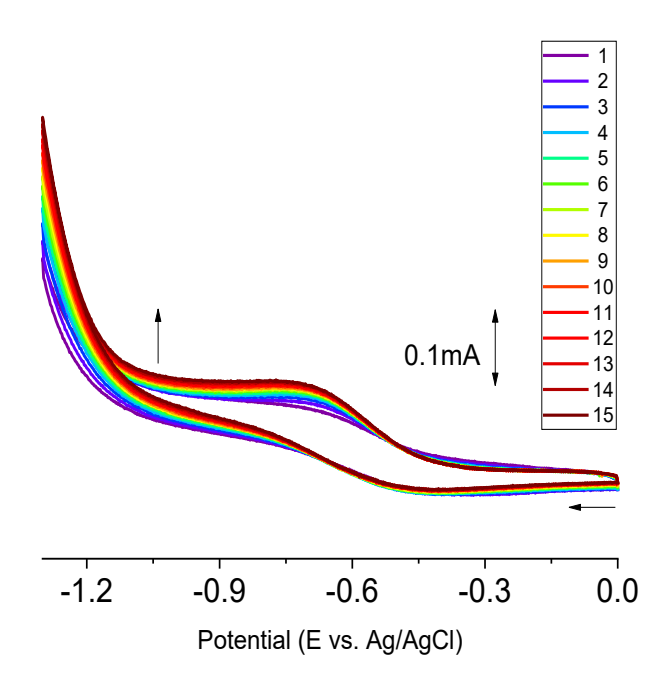


Figure 6. Multi-cyclic voltammograms of $VO_{0.3}N_{0.7}$ oxynitride film in N_2 -saturated solution. The arrow gives the trend of cathodic current upon repeated cycling. Scan rate = 100 mV s^{-1} .

catalytic activity. AFM data acquired after the repeated potential cycling (Figure 6), however, showed negligible changes in surface roughness, with an estimated RMS roughness of 31 nm determined from AFM measurements. (See Supporting Information, Figure S1).

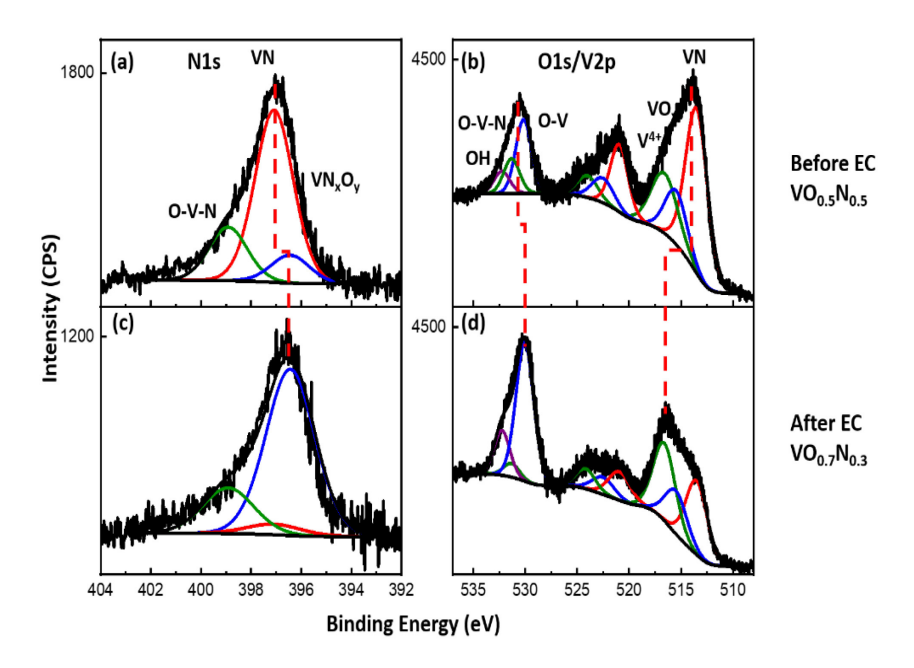


Figure 7. (a) N 1s and (b) O 1s/V 2p spectra for a $VO_{0.5}N_{0.5}$ film after deposition but prior to electrochemical measurements: (c) and (d); corresponding data after emersion from N₂-saturated Na₂SO₄ electrolyte (pH = 7) at -1.6 V vs. Ag/AgCl. Dashed lines are guides to the eye. Note that this film is distinct from the film used to obtain the data plotted in Figure 6.

XPS data (Figures 7 and 8), however, acquired prior to and after electrochemical polarization of separate vanadium oxynitride films (emersion at -1.6 V vs. Ag/AgCl) demonstrate that the process of cathodic polarization at pH 7 induces significant changes to the oxynitride surface structure. In both the presence (Figure 7a, c) and absence (Figure 8a, c) of dissolved N₂, the N 1s peak maximum shifts from ~ 397.1 eV to 396.5 eV. For both films, the V 2p spectrum (Figure 7b, d; 8b, d) shifts toward higher binding energies, indicative of oxidation.²⁴ In Figure 7c (N₂-saturated solution) there is a pronounced V 2p_{3/2} maximum near 516 eV binding energy, indicative of V(IV) formation.^{24,36} A similar, though less pronounced, shift is also observed in Ar-saturated solution (Figure 8c). Both Figures 7c and 8c show that O 1s intensity significantly increased after cathodic polarization. In both the presence and absence of dissolved N₂, the films after cathodic polarization exhibit a significant increase in relative O/N atomic ratio. The data in Figures 7 and 8, therefore, demonstrate that vanadium oxynitride films, upon cathodic polarization, exhibit a shift in the N 1s spectrum from ~397.0 eV towards 396.5 eV, coincident with additional oxidation of the oxynitride surface region. These XPS binding energy shifts occur in both the presence and absence of N₂

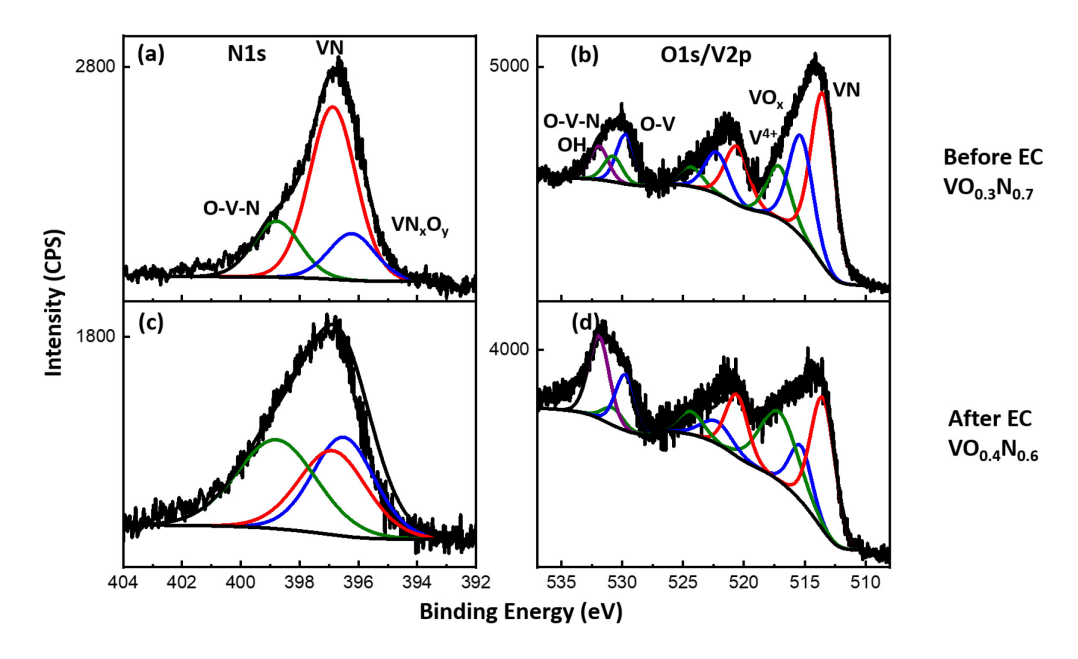


Figure 8. (a) N 1s and (b) O 1s/V 2p XPS spectra for a VO_{0.3}N_{0.7} film after deposition but prior to electrochemical measurements: (c) and (d); corresponding data after emersion from Ar-saturated 0.1 M Na₂SO₄ electrolyte (pH 7) at -1.6 V vs. Ag/AgCl.

XPS data acquired after multi-cyclic polarization (Figure 6) and emersion at -1.3 V vs. Ag/AgCl are displayed in Figure 9. The slight shift of the N 1s feature to lower binding energies (see above) is still apparent (Figure 9a, c), although emersion at somewhat less cathodic potential yields smaller changes in the V $2p_{3/2}$ spectrum (Figure 9b, d). Notable, however, is the sharp decrease in N/O atomic ratio, from N/O ~ 2 to N/O ~ 1, This is consistent with the data in Figures 7 and 8, indicating that cathodic polarization, in the absence or presence of N₂ results in depletion of lattice N within the XPS sampling depth, estimated here as twice the inelastic mean free path of the N 1s electron, or ~ 20 Å. These results are also consistent with those previously reported for vanadium oxynitride nanoparticles. ¹²

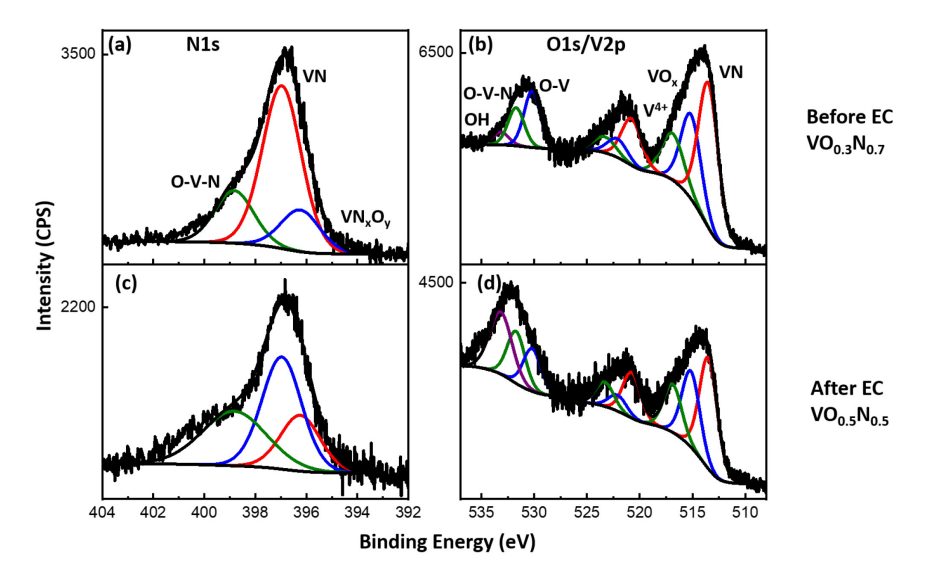


Figure 9. (a) N 1s and (b) O 1s/V 2p XPS spectra for a VO_{0.3}N_{0.7} film after deposition but prior to electrochemical measurements (the same film as in Figure 6): (c) and (d); corresponding data after emersion from N₂-saturated 0.1 M Na₂SO₄ electrolyte (pH 7) at -1.3 V vs. Ag/AgCl.

Given the exposure of the oxynitride films (Figures 7 - 9) to ambient immediately upon emersion from the electrolyte, caution must be exercised in the interpretation of the subsequently-acquired XPS spectra. However, it is notable that XPS N 1s, O 1s, and V 2p binding energy shifts as shown in Figures 7 - 9 were previously reported upon O₂ plasma oxidation of vanadium oxynitride films with film transfer from the plasma chamber to the XPS analysis chamber carried out in-situ.²³ Such a change upon O₂ plasma oxidation is shown, for the convenience of the reader, in Figure S3 of Supporting Information. Thus, the changes to N 1s and O 1s/V 2p core-level spectra shown in Figures 7 - 9 can be observed (albeit produced by different methods) in the presence or absence of ambient exposure. In this respect, it is also important to note that such changes to core-level spectra cannot be produced by O₂ exposure at or above room temperature.²⁴ We have also exposed vanadium oxynitride films to H₂O vapor at 300 K, at partial pressures < 10⁻⁵ Torr, without any evidence of significant change in the N 1s, O 1s or V 2p spectra. Therefore, one cannot ascribe the changes to core-level spectra displayed in Figures 7 - 9 to exposure to ambient. The changes observed instead reflect changes to the oxynitride surface structure induced by cathodic polarization in the electrolyte.

Comparing Vanadium Oxynitride and Vanadium Oxide Films

We have previously demonstrated that N-vacant vanadium oxide films with mixed V(III)/V(IV) surface states can reduce N₂ to NH₃ at pH 7.¹⁴ Electrochemical polarization curves at cathodic voltages for such an N-vacant vanadium oxide film and for a VO_{0.4}N_{0.6} film are compared in Figure 10a. The data in Figure 10a. demonstrate higher total activity and an earlier onset potential for the N-vacant vanadium oxide film relative to the oxynitride film in the N₂-saturated solution. The higher activity could mainly pertain to a competing HER in addition to NRR.

The absorbance spectrum of indophenol blue from NH₃ produced by controlled potential bulk electrolysis in the presence of N₂ is also shown in Figure 10b, indicating a similar NRR activity for both films under a nitrogen environment. This suggestion is corroborated by data in Table I, comparing onset potentials and calculated FEs for the N-vacant vanadium oxide (VO_x) and for the vanadium oxynitride (VO_{0.4}N_{0.6}) film. Onset potentials have been converted to RHE to facilitate comparison to other results in the literature. These data demonstrate earlier onset potentials for the VO_x film in both N₂ and Ar-saturated solutions. However, the FE in the N₂-saturated solution is somewhat higher for the VO_{0.4}N_{0.6} film versus the VO_x film, consistent with the reduction of both lattice N and N₂ in the former film. Additionally, the FE determined for the vanadium oxynitride film in N₂-saturated solution is approximately twice that measured in Ar-saturated solution. This corroborates the above finding that, in the presence of N₂ at pH 7, both N₂ and lattice N are being reduced to NH₃. In comparing FEs for vanadium oxynitride films in Table I to higher values published in the literature, 12, 13 it should be noted that the data in Table I were (a) recorded on flat films with far lower surface areas than the nanoparticles previously examined, and (b) that the data in Table I were acquired at pH 7, rather than at pH 1, which was the environment for the nanoparticle studies.

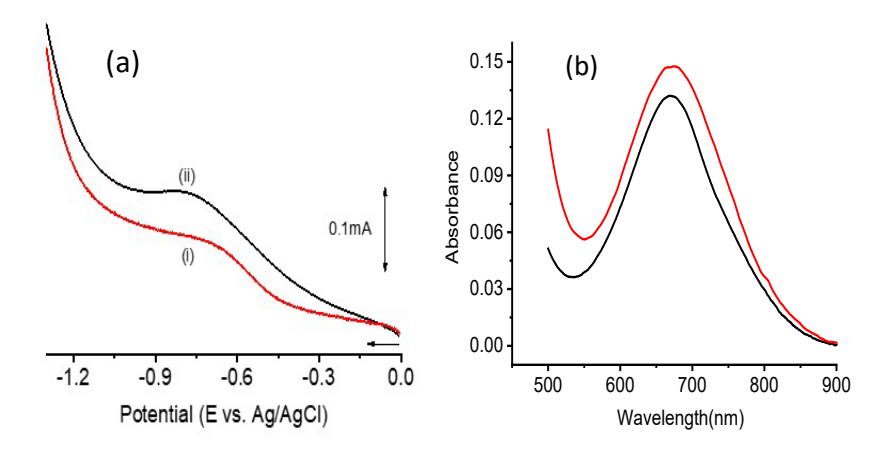


Figure 10. (a) Comparison of EC polarization curves for (i) VO_{0.4}N_{0.6} film on FTO (red trace), and (ii) N-free VO_x film on FTO (black trace in N₂-saturated 0.1 M Na₂SO₄ at pH 7). (b) Absorbance spectrum of indophenol blue from NH= produced by controlled potential bulk electrolysis of (i) VO_{0.4}N_{0.6} film (black trace), (ii) N-free VO_x film (red trace).

Also of interest in Table I is the finding of a Faradaic Efficiency of 0.06% for an N-vacant vanadium oxide film in Ar-saturated solution. This obviously marks the limits of precision in the determination of NH₃ production for these films under these conditions. Additionally, the onset potential for each film remains unchanged in either N₂-saturated or Ar-saturated solution, demonstrating that non-NRR pathways (likely HER) dominate electrochemical activity at these lower potentials, even at pH 7. However, the higher currents observed for the VO_x film in Figure 10a suggest relatively.

TABLE I. Summary of Faradaic Efficiencies and Onset potentials for lattice N vs N_2 reduction at vanadium oxynitride and vanadium oxide surfaces. Faradaic Efficiencies were measured at -0.7 V vs. Ag/AgCl (= -0.49 V vs. RHE) for all films. The VO_{0.4}N_{0.6} film is the same as in Figure 10.

Catalyst	Conditions	Onset Potential, V vs. RHE	Faradaic Efficiency
VO _{0.4} N _{0.6}	N ₂	-0.060	0.37%
	Ar	-0.060	0.11%
V/VO_x	N_2	0.045	0.26%
	Ar	0.045	0.06%

higher contributions from HER on this electrode surface compared to that on the VO_xN_y surface.

The different rates of reduction of lattice N and of N₂ to NH₃ for vanadium oxynitride films are evidence that they proceed by parallel but separate mechanisms, rather than by a Mars-Van Krevelen-type mechanism (MVK), in which N₂ is first incorporated into the film lattice, and then reduced to NH₃. Consistent with this proposal, XPS measurements of the N-vacant vanadium oxide films after emersion from N₂-saturated electrolyte at -1.6 V vs. Ag/AgCl found no evidence of N incorporation into the oxide lattice (Figure S5, Supporting Information). The absence of any XPS evidence of N incorporation, combined with a large difference in measured reduction rates at the same potential, argues strongly against an MVK-type mechanism for vanadium oxynitride films under these experimental conditions.

Theory: [V]_O vs. [V]_N sites

The experimental data presented above indicate that the reduction pathways for lattice N and dissolved N_2 are distinct, but both involve reactions at $[V]_0$ sites. Previous calculations concerning N_2 interactions with transition metal cation sites have shown that dissociation of metal-bound N_2 to $M\equiv N$: (Eq. 1 generalized to other metals) is energetically favored at $[M]_0$ sites over $[M]_N$ sites for oxophilic metals (M=V, Ti) but less so for less oxophilic metals, such as $Cr.^{14}$ Such unsaturated intermediates have previously been proposed as part of a dissociative NRR reaction pathway³⁷ Our previous theoretical results regarding Eq. (2) do not, however, address other potential intermediate pathways, including possible protonation of surface-bound N_2 .

To examine further the possible roles of $[V]_0$ and $[V]_N$ centers in supporting possible reaction pathways for the reduction of N_2 , DFT-based calculations were carried out for a variety of putative N/H reaction intermediates³⁷ at both $[V]_0$ and $[V]_N$ centers. Selected $[V]_0$ -N_aH_b (a = 1 or 2, b = 1, 2 or 3) surface configurations are shown schematically in Figure 11. Calculated free energies for these configurations—relative to surface bound N_2 —are compared in Figure 11 for E (ligand) = O (red) or N (blue).

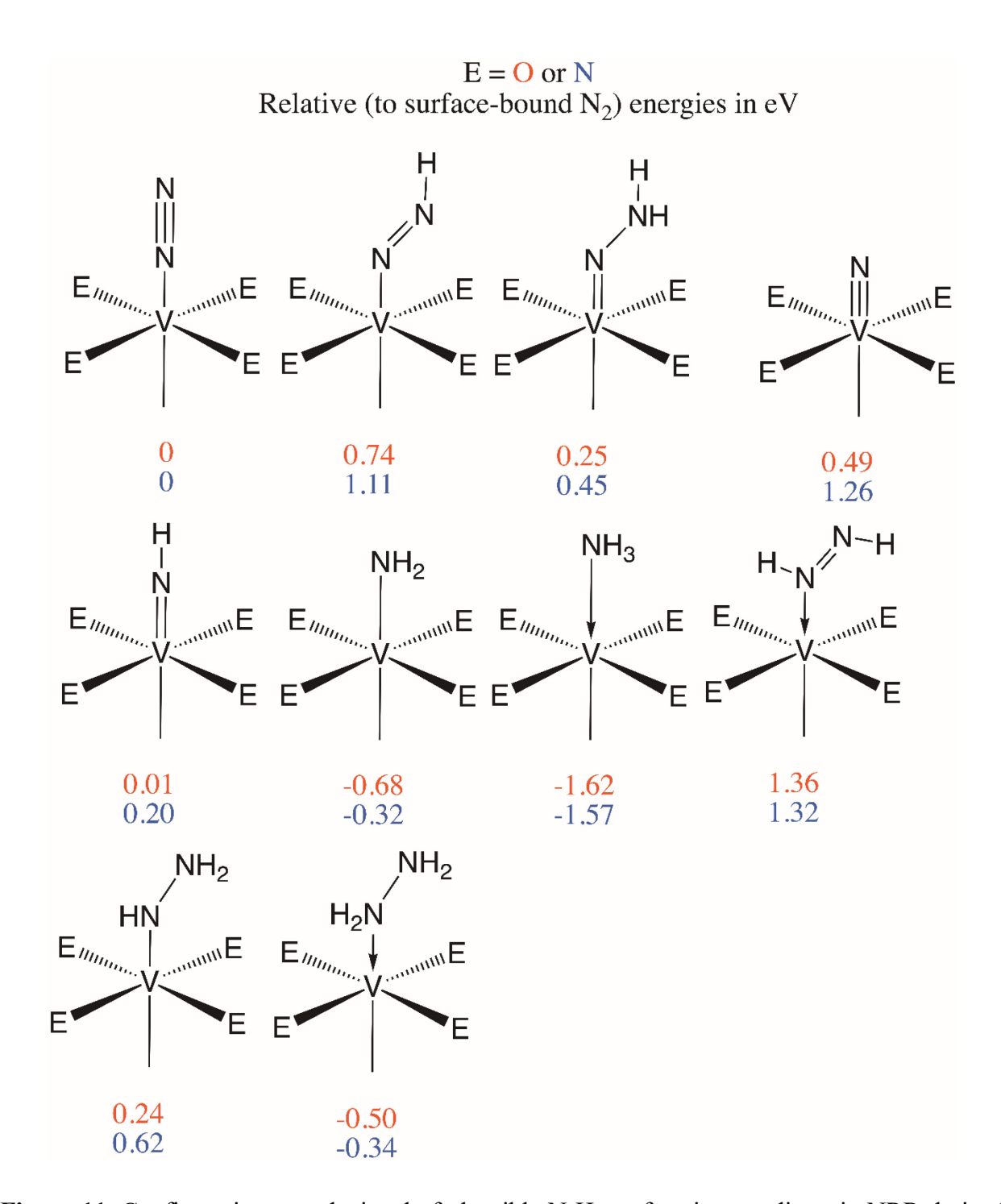


Figure 11. Configurations are depicted of plausible N_xH_y surface intermediates in NRR derived from plane-wave DFT simulations. Free energies (in eV) – shown below each structure – are calculated relative to that of surface bound N_2 for both E = O (red), $[V]_O$, and E = N (blue), $[V]_N$.

The data in Figure 11 demonstrate that the formation of the V \equiv N: complex from molecularly adsorbed N₂ (reaction 1) is energetically favored at [V]₀ vs [V]_N sites by ~ 0.8 eV, i.e., E_{rel} = 0.49

eV ([V]₀=N:) vs. 1.26 eV [V]_N=N:). Optimized geometries for [V]₀=N: and [V]_N=N:, however, are remarkably similar, as shown in Figure 12. The reason for the lower calculated energy at the [V]₀ site is therefore not immediately apparent. We speculate that the greater electronegativity of the O ligands induces a lower initial electron charge density at the vanadium cation site, thus favoring the Lewis base adsorption. The data in Figures 11 and 12, however, do show that V=N: formation—indicated as a reaction intermediate for lattice N reduction (e.g., XPS data, Figures 7-9) is energetically favored by ~0.8 eV at [V]₀ sites, in agreement with the XPS data.

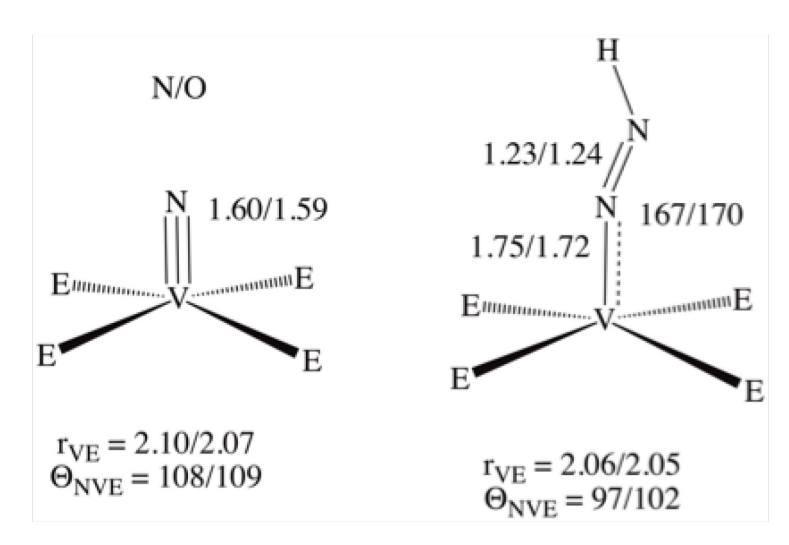


Figure 12. Optimized core geometries of surface configurations from plane-wave DFT calculations for V-nitride (left) and V-diazenide (right) for [V]_N / [V]_O centers. Bond distances are in Angstrom units; bond angles in degrees. See Figures S6 and S7 for three-dimensional representations of these surface configurations.

In contrast to lattice N reduction, there is no experimental evidence for a specific intermediate in the reduction of dissolved N₂ to NH₃ at vanadium oxide or oxynitride surfaces. For these systems, however, the diazenide complex (V-N=NH) is a plausible intermediate representing the initial protonation step.³⁷ As shown in Figure 11, diazenide formation from V-N₂ is energetically favored at [V]₀ vs. [V]_N sites by almost 0.5 eV, yet optimized diazenide geometries at [V]₀ vs. [V]_N sites (Figure 12) are very similar. The reasons for the difference in diazenide stabilization energies were therefore further probed by borrowing from analyses in the PCET (proton-coupled electron transfer) literature.³⁸ First, the energetics of proton addition to [V]-NN were computed. Second, an electron was added to [V]-NN, and the energy of this transfer was computed. While

the calculation of accurate energies likely requires simulation of solvent effects, energy differences between related chemical models are expected to be reliable. ³⁸ Interestingly, for the ET process, the computed energies differ by only 0.1 eV, suggesting that reduction of each surface-bound dinitrogen is roughly similar in energy at [V]o and [V]_N sites. There is, however, a more noticeable difference in the protonation energies between the N- and O-rich surface dinitrogen models, as shown in Figure 13. Protonation was computed to be favorable by 4.35 eV for the [V]o-NN model and downhill by 3.93 eV for the [V]_N-NN model (Figure 13). This corresponds to a difference of 0.4 eV in favor of the O-rich [V]o oxynitride surface model, a value that is commensurate with the computed relative energy difference between the two [V]-NNH surface states. The calculations thus suggest that the difference in the stability in the diazenide surface states is a consequence of the greater ease of protonation of surface-bound N₂ for the O-rich model than for the N-rich surface model, suggesting greater Lewis acidity of the vanadium binding site when it is ligated by more electronegative O atoms. Given the similar relative stability of diazenide ([V]-NNH, $\delta E_{\rm ON} \sim 0.37$ eV) and hydrazide ([V]-NHNH2, $\delta E_{\rm ON} \sim 0.38$ eV, Figure 11), we hypothesize a similar origin to the stability difference of the latter intermediates.

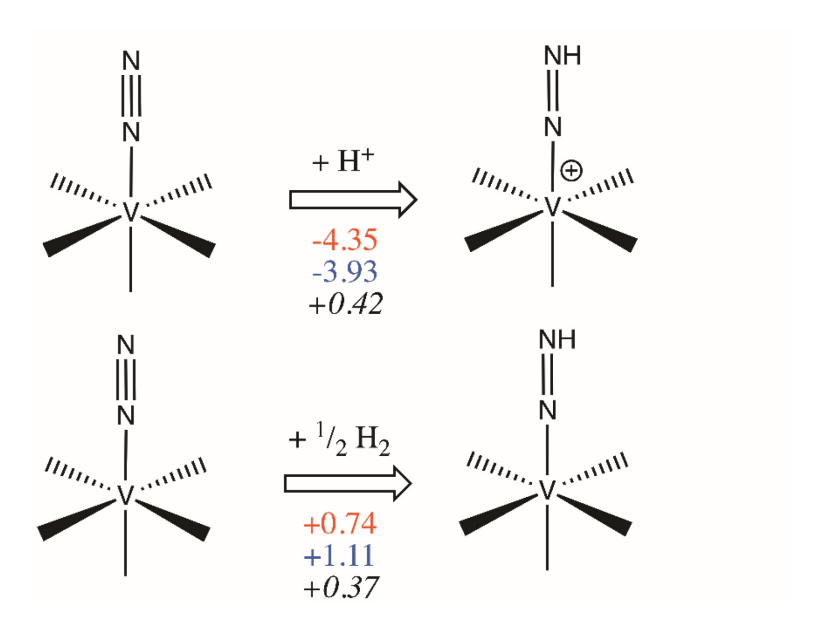


Figure 13. DFT-calculated energies to add a proton (top) or a hydrogen atom (i.e., $\frac{1}{2}$ H₂) to a bound dinitrogen for two V-oxynitride surface models. The energies (in eV) are quoted for an Orich surface model, [V]₀, in red font, an N-rich surface model, [V]_N, in blue font, and the difference between the two surface models (italics font). The similarity in the difference for the [V]₀ and

[V]_N models implies that the differences in the stability of the diazenido states, [V]-NNH, is due to the proton affinity of the surface-bound dinitrogen as opposed to differences in ease of reduction.

DISCUSSION

The experimental data presented here clearly demonstrate that (a) V-oxynitride films can produce NH₃ during cathodic polarization even in Ar-purged solution, and that (b) N₂ reduction occurs at N-vacant vanadium oxides without evidence of N incorporation into the lattice. These data indicate that the reduction of lattice N and the reduction of dissolved N₂ occur by different mechanisms rather than by a single MVK mechanism. An MVK mechanism was proposed for NRR of vanadium oxynitride nanoparticles based on ion exchange studies showing that for ¹⁵N₂, both ¹⁵NH₃ and ¹⁴NH₃ formation were observed under acidic conditions. ^{7,13} Similar conclusions were also reported for Ti oxynitrides. ³⁹ It should be pointed out, however, that parallel reduction pathways for lattice N and N₂ discussed above would yield the same results for such ion-exchange experiments. The evidence presented here therefore strongly suggests that, for vanadium oxynitride films, an MVK mechanism is not operative.

The XPS data in Figures 7 - 9 demonstrate that cathodic polarization of vanadium oxynitride in the presence or absence of N₂—results in the formation of V≡N: or similar unsaturated VN surface states supported on a thin V(III)/V(IV) oxide overlayer. Such states are present at the surfaces of vanadium oxynitride nanoparticles, and the diminution of this feature's intensity (in ex situ XPS) correlates with the diminution of NRR activity. 12 The evidence, therefore, indicates that such unsaturated VN configurations are indeed intermediates in the reduction of lattice N to NH₃. The DFT calculations indicate an energetic stabilization of V≡N: at [V]_O vs. [V]_N sites by ~0.8 eV (Figure 11), which also explains why the formation of such surface states is associated with the formation of a thin oxide overlayer at the surface of the oxynitride films. The fact that such transformations at vanadium oxynitride surfaces are observed upon O₂ plasma oxidation, ²² but not by O₂ thermal oxidation,²⁴ suggests an underlying similarity in plasma and electrochemically induced oxidation mechanisms for vanadium oxynitride surfaces. Indeed, O2 plasma treatment of a VO_{0.3}N_{0.7} film (Figure S3, Supporting Information), resulting in XPS spectra very similar to those displayed in Figs 7c, d and 8c, d —resulted in only a slight increase in cathodic activity in N₂-saturated solution (Figure S4, Supporting Information). Further, the electrochemical behavior remains stable upon repeated cycling (Figure S4, Supporting Information). Thus, O₂ plasma

oxidation and electrochemical cathodic polarization produce similar surface structures with similar NRR activity.

Experimental data (Figure 1 - 10 and Table I) and theoretical results (Figures 11 - 13) demonstrate that N₂ adsorption and subsequent protonation are also energetically favored at [V]o sites rather than at [V]_N sites. The data suggest that, for other metals with high oxophilicity,⁴⁰ a similar relationship should exist. Indeed, for example, Ti, V, and Nb, pure nitride phases are NRR inactive.^{39,41} In contrast, NbO₂ nanoparticles have been reported to exhibit relatively high NRR activity with 32% Faradaic Efficiencies.⁴² These observations for oxophilic metals suggest that the consistent energetic stabilization of plausible reaction intermediates at [V]o vs. [V]_N centers (Figure 10) reflects a lower initial valence electron charge density at [V]o centers. Thus, for oxophilic metals, oxynitrides may be a route toward storing N for NRR under some circumstances. It must be emphasized, however, that these data do not indicate the relative selectivities of oxophilic oxynitrides vs. corresponding oxides for NRR over competitive reaction pathways, including HER.

SUMMARY AND CONCLUSION

Theory and experiment have been integrated to understand fundamental mechanisms of NRR at the surfaces of V oxynitride films under pH 7 conditions. The films were formed by magnetron sputter deposition on FTO substrates, and characterized by XRD, AFM, electrochemistry, ex situ XPS and plane-wave DFT calculations. The polycrystalline films exhibited NRR activity, with NH3 evolution detected in both Ar-saturated and N2-saturated solutions. This demonstrates that the reduction of lattice N to NH3 can occur in both the absence and presence of N2. Ex situ XPS measurements in both cases indicate that, within the estimated XPS sampling depth (ca. twice the approximate inelastic mean free path of N 1s electrons, 32 or 3 nm), cathodic polarization under these conditions coincides with a shift in the N 1s peak binding energy from ~ 397.1 eV to 396.5 eV, as well as formation of a thin oxide overlayer.

The N 1s feature at 396.5 eV has been correlated with NRR activity in V (and Ti) oxynitrides, 12,13,39 and has been identified by theory and experiment as indicative of V \equiv N: or similar unsaturated VN surface state on top of the V oxide overlayer. 23 The data reported here, in conjunction with previous reports, 14 indicate that lattice N in V oxynitride films can be reduced to NH₃ in the presence or absence of N₂, and that a reaction intermediate in this process is an

unsaturated VN surface state, which theory and experiment suggest is $V \equiv N$: That such intermediates are formed in conjunction with a thin oxide overlayer is evidence that this process occurs preferentially at $[V]_0$, rather than at $[V]_N$ cationic V surface cations.

Similar experiments on N-free vanadium oxide films under identical conditions demonstrate the formation of NH₃ from N₂ without observable incorporation of N into the oxide lattice. Thus, N₂ reduction to NH₃ occurs without formation of lattice N, and lattice N is reduced in the presence or absence of N₂ via formation of a V \equiv N: or similar surface state. This indicates separate, distinct mechanisms for the reduction of N₂ and lattice N in V oxynitrides. Both reduction mechanisms are also energetically favored at [V]₀, rather than at [V]_N sites.

Experimental studies are closely corroborated by DFT-based calculations showing that the formation of a variety of possible NRR reaction intermediates are consistently energetically favored at [V]₀, rather than at [V]_N sites. These studies also indicate that a major factor in the energetic favoring of [V]₀ centers is the protonation of bound N₂, rather than electron transfer to the protonated species, consistent with a lower valence electron density at [V]₀ centers. These calculations, in conjunction with previous theoretical results, ¹⁴ suggest similar conclusion for other oxophilic metal systems, such as Ti oxynitride, but perhaps not for the oxides and nitrides of less oxophilic metals, such as Cr or Co.

The experimental and theoretical findings presented here indicate that the broadly accepted MVK mechanism^{7,13,39} does not occur for V oxynitrides under these experimental conditions. These findings—that N₂ and lattice N are reduced to NH₃ by separate mechanisms, occurring preferentially at [V]o sites—are also consistent with the results of the N isotope exchange studies¹³ which formed the basis for the hypothesis of an MVK mechanism. Such a conclusion, of course, impacts how one views oxynitrides vs. oxides as NRR catalysts. Caution should be exercised, however, as the data presented here do not allow one to conclude how the presence of lattice N might alter, e.g., selectivity towards NRR vs. HER at various pH values.

Finally, it is of interest to note that the formation of V/N surface states with binding energies of 396.5 eV, coincident with formation of a thin surface oxide layer, occurs by cathodic polarization and not by exposure to ambient (Figures 7 - 9). Such changes cannot be induced by thermal oxidation,²⁴ but are exactly reproduced upon exposure of a clean vanadium oxynitride surface to an O₂ plasma.²³ This suggests a fundamental relationship between oxidation mechanisms in the electrocatalytic and plasma environments. This, and broader questions of

surface oxynitride structure/function relationships as a function of electrochemical potential and

pH are currently being explored in our laboratories and will be the subjects of future publications.

ASSOCIATED CONTENT

Supporting Information.

The Supporting Information is available free of charge on the ACS Publications website at

DOI: 10.1021/acsami.xxxx. This section contains (Figure S1) optical and atomic force microscopy

of a vanadium oxynitride film after cyclic polarization in N2-saturated electrolyte; (Figure S2)

Electrochemical measurements of the vanadium oxynitride film surface area; (Figure S3) N 1s and

O 1s/V 2p XPS spectra of a vanadium oxynitride film before and after O₂ plasma oxidation; (Figure

S4) and cathodic polarization curves for a vanadium oxynitride film before and after such plasma

treatment, in a N2-saturated 0.1 M Na₂SO₄ solution at pH 7; (Figure S5) XPS data indicating a lack

of N incorporated in a vanadium oxide film used to reduce dissolved N₂ at pH 7; 3D representations

of nitride (Figure S6) and diazenide (Figure S7) surface configurations (PDF).

AUTHOR INFORMATION

Corresponding Authors

E-mail and ORCID

Thomas.Cundari@unt.edu, ORCID: 0000-0003-1822-6473

Francis.DSouza@unt.edu; ORCID: 0000-0003-3815-8949

Jeffry.Kelber@unt.edu, ORCID: 0000-0002-3259-9068

Contributing Authors

Adaeze Osonkie

Ashwin Ganesan

Precious Chukwunenye

Fatima Anwar

Kabirat Balogun

Mojgan Gharee

25

Ishika Rashed

Author Contributions

The manuscript was written through contributions of all authors. All authors have given approval to the final version of the manuscript.

Notes

The authors declare no competing financial interest

ACKNOWLEDGEMENTS

The authors gratefully acknowledge the support of this work by the National Science Foundation through grants DMR-2112864 (to JAK, TRC and FD) and partial support by CHE-1953547 (to TRC). Additional NSF support for the UNT CASCaM HPC cluster via Grant CHE-1531468 is also gratefully acknowledged. Partial support to initiate this research was also provided by UNT through the Office of the Vice President for Research, the College of Science and the Department of Chemistry and is gratefully acknowledged. Dr. Slavomir Nemšák (LBNL) is also acknowledged for stimulating discussions.

REFERENCES

- (1) Qing, G.; Ghazfar, R.; Jackowski, S. T.; Habibzadeh, F.; Ashtiani, M. M.; Chen, C.; Smith, M. R.; Hamann, T. W. Recent Advances and Challenges of Electrocatalytic N₂ Reduction to Ammonia. *Chem. Rev.* **2020**, *120*, 5437-5516.
- (2) Zang, W.; Yang, T.; Zou, H.; Xi, S.; Zhang, H.; Liu, X.; Kou, Z.; Du, Y.; Feng, Y. P.; Shen, L.; Duan, L.; Wang, J.; Pennycook, S. J. Copper Single Atoms Anchored in Porous Nitrogen-Doped Carbon as Efficient pH-Universal Catalysts for the Nitrogen Reduction Reaction. *ACS Catal.* **2019**, *9*, 10166-10173.
- (3) Lin, Y.; Zhang, S.; Xue, Z.; Zhang, J.; Su, H.; Zhao, T.; Zhai, G.; Li, X.; Antonietti, M.; Chen, J. Boosting Selective Nitrogen Reduction to Ammonia on Electron-Deficient Copper Nanoparticles. *Nat. Commun.* **2019**, *10*, 4380(1-7).

- (4) Han, L.; Ren, Z.; Ou, P.; Cheng, H.; Rui, N.; Lin, L.; Liu, X.; Zhuo, L.; Song, J.; Sun, J.; Luo, J.; Xin, H. L. Modulating Single-Atom Palladium Sites with Copper for Enhanced Ambient Ammonia Electrosynthesis. *Angew. Chem. Int. Ed.* **2021**, *60*, 345-350.
- (5) Manjunatha, R.; Karajić, A.; Goldstein, V.; Schechter, A. Electrochemical Ammonia Generation Directly from Nitrogen and Air Using an Iron-Oxide/Titania-Based Catalyst at Ambient Conditions. *ACS Appl. Mater. Interfaces* **2019**, *11*, 7981-7989.
- (6) Wang, T.; Liu, Q.; Li, T.; Lu, S.; Chen, G.; Shi, X.; Asiri, A. M.; Luo, Y.; Ma, D.; Sun, X. A Magnetron Sputtered Mo₃Si Thin Film: An Efficient Electrocatalyst for N₂ Reduction under Ambient J. Mater. Chem. A, 2021, 9, 884-888
- (7) Qiao, Z.; Johnson, D.; Djire, A. Challenges and Opportunities for Nitrogen Reduction to Ammonia on Transitional Metal Nitrides via Mars-van Krevelen Mechanism. *Cell Rep.* **2021,** *2*, 100438.
- (8) Liu, Q.; Xu, T.; Luo, Y.; Kong, Q.; Li, T.; Lu, S.; Alshehri, A. A.; Alzahrani, K. A.; Sun, X. Recent Advances in Strategies for Highly Selective Electrocatalytic N₂ Reduction toward Ambient NH₃ Synthesis. *Curr. Opin. Electrochem.* **2021**, *29*, 100766 (1-18).
- (9) Xu, T.; Ma, B.; Liang, J.; Yue, L.; Liu, Q.; Li, T.; Zhao, H.; Luo, Y.; Lu, S.; Sun, X. Recent Progress in Metal-Free Electrocatalysts toward Ambient N₂ Reduction Reaction. *Acta Phys. Chim. Sin.* **2021**, *37*, 2009043.
- (10) Qu, X.; Shen, L.; Mao, Y.; Lin, J.; Li, Y.; Li, G.; Zhang, Y.; Jiang, Y.; Sun, S. Facile Preparation of Carbon Shells-Coated O-Doped Molybdenum Carbide Nanoparticles as High Selective Electrocatalysts for Nitrogen Reduction Reaction under Ambient Conditions. *ACS Appl. Mater. Interfaces* **2019**, *11*, 31869-31877.

- (11) Nash, J.; Yang, X.; Anibal, J.; Dunwell, M.; Yao, S.; Attenkofer, K.; Chen, J. G.; Yan, Y.; Xu, B. Elucidation of the Active Phase and Deactivation Mechanisms of Chromium Nitride in the Electrochemical Nitrogen Reduction Reaction. *J. Phys. Chem. C* **2019**, *123*, 23967-23975.
- (12) Yang, X.; Nash, J.; Anibal, J.; Dunwell, M.; Kattel, S.; Stavitski, E.; Attenkofer, K.; Chen, J. G.; Yan, Y.; Xu, B. Mechanistic Insights into Electrochemical Nitrogen Reduction Reaction on Vanadium Nitride Nanoparticles. *J. Am. Chem. Soc.* **2018**, *140*, 13387.
- (13) Yang, X.; Kattel, S.; Nash, J.; Chang, X.; Lee, J.; Yan, Y.; Chen, J.; Xu, B. Quantification of Active Sites and Elucidation of Reaction Mechanism of Electrochemical Nitrogen Reduction Reaction on Vanadium Nitride. *Angew. Chem. Int. Ed.* **2019**, *58*, 13768-13772.
- (14) Ganesan, A.; Osonkie, A.; Chukwunenye, P.; Rashed I.; Cundari, T. R.; D'Souza, F.; Kelber, J. A. Electrochemical Reduction of N₂ to Ammonia by Vanadium Oxide Thin Films at Neutral pH: Oxophilicity and the NRR Reaction. *J. Electrochem. Soc.* **2021**, *168*, 026504.
- (15) Pan, J; Anton, H. A.; Vegge, T. Vanadium Oxynitrides as Stable Catalysts for Electrochemical Reduction of Nitrogen to Ammonia: the Role of Oxygen. *J. Mater. Chem. A.* **2020,** *8*, 24098-24107.
- (16) Garrick, T. R.; Diao, W.; Tengco, J. M.; Stach, E. A.; Senanayake, S. D.; Chen, D. A.; Monnier, J. R.; Weidner, J. W. The Effect of the Surface Composition of Ru-Pt Bimetallic Catalysts for Methanol Oxidation. *Electrochim. Acta* **2016**, *195*, 106-111.
- (17) Faisal, F.; Stumm, C.; Bertram, M.; Waidhas, F.; Lykhach, Y.; Cherevko, S.; Xiang, F.; Ammon, M.; Vorokhta, M.; Šmíd, B.; Skála, T.; Tsud, N.; Neitzel, A.; Beranová, K.; Prince, K. C.; Geiger, S.; Kasian, O.; Wähler, T.; Schuster, R.; Schneider, M. A.; Matolín, V.; Mayrhofer, K. J. J.; Brummel, O.; Libuda, J.; Electrifying Model Catalysts for Understanding Electrocatalytic Reactions in Liquid Electrolytes. *Nat. Mater.* **2018**, *17*, 592-598.

- (18) Spurgeon, P. M.; Liu, D.; Windus, T. L.; Evans, J. W.; Thiel, P. A. Enhanced Nanostructure Dynamics on Au(111) with Adsorbed Sulfur due to Au–S Complex Formation. *ChemPhysChem* **2021**, *22*, 349-358.
- (19) Ali-Löytty, H.; Louie, M. W.; Singh, M. R.; Li, L.; Sanchez Casalongue, H. G.; Ogasawara, H.; Crumlin, E. J.; Liu, Z.; Bell, A. T.; Nilsson, A.; Friebel, D. Ambient-Pressure XPS Study of a Ni–Fe Electrocatalyst for the Oxygen Evolution Reaction. *J. Phys. Chem. C* **2016**, *120*, 2247-2253.
- (20) Karsliğlu, O.; Nemšák, S.; Zegkinoglou, I.; Shavorskiy, A.; Hartl, M.; Salmassi, F.; Gullikson, E. M.; Ng, M. L.; Rameshan, C.; Rude, B.; Bianculli, D.; Cordones, A. A.; Axnanda, S.; Crumlin, E. J.; Ross, P. N.; Schneider, C. M.; Hussain, Z.; Liu, Z.; Fadley, C. S.; Bluhm, H. Aqueous Solution/Metal Interfaces Investigated in operando by Photoelectron Spectroscopy. *Faraday Discuss.* **2015**, *18*, 35-53.
- (21) Pfaff, S.; Larsson, A.; Orlov, D.; Harlow, G. S.; Abbondanza, G.; Linpé, W.; Rämisch, L.; Gericke, S. M.; Zetterberg, J.; Lundgren, E. Operando Reflectance Microscopy on Polycrystalline Surfaces in Thermal Catalysis, Electrocatalysis, and Corrosion. *ACS Appl. Mater. Interfaces* **2021**, *13*, 19530-19540.
- (22) Källquist, I.; Lindgren, F.; Lee, M.; Shavorskiy, A.; Edström, K.; Rensmo, H.; Nyholm, L.; Maibach, J.; Hahlin, M. Probing Electrochemical Potential Differences over the Solid/Liquid Interface in Li-Ion Battery Model Systems. *ACS Appl. Mater. Interfaces* **2021**, *13*, 32989.
- (23) Osonkie, A.; Lee, V.; Chukwunenye, P.; Cundari, T.; Kelber, J. Plasma Modification of Vanadium Oxynitride Surfaces: Characterization by *in-situ* XPS Experiments and DFT Calculations. *J. Chem. Phys.* **2020**, *153*, 144709
- (24) Glaser, A.; Surnev, S.; Netzer, F. P.; Fateh, N.; Fontalvo, G. A.; Mitterer, C. Oxidation of Vanadium Nitride and Titanium Nitride Coatings. *Surf. Sci.* **2007**, *601*, 1153-1159

- (25) Hafner, J.; Kresse, G. The Vienna AB-Initio Simulation Program VASP: An Efficient and Versatile Tool for Studying the Structural, Dynamic, and Electronic Properties of Materials. *In Properties of Complex Inorganic Solids, Gonis A., Meike A., Turchi P.E.A. (eds), pp 69-82, Springer, Boston, MA, 1997.*
- (26) Monkhorst, H. J.; Pack, J. D. Special Points for Brillouin-Zone Integrations. *Phys. Rev. B* **1976,** *13*, 5188-5192.
- (27) Methfessel, M.; Paxton, A. T. High-precision Sampling for Brillouin-Zone integration in Metals. *Phys. Rev. B Condens. Matter* **1989**, *40*, 3616-3621.
- (28) Osonkie, A.; Lee, V.; Oyelade, A.; Mrozek-McCourt, M.; Chukwunenye, P.; Golden, T. D.; Cundari, T. R.; Kelber, J. A. Chemical and Electronic Structures of Cobalt Oxynitride Films Deposited by NH₃ vs. N₂ Plasma: Theory vs. Experiment. *Phys. Chem. Chem. Phys.* **2020**, *22*, 2464-24648.
- (29) Sangiovanni, D. G.; Mei, A. B.; Hultman, L.; Chirita, V.; Petrov, I.; Greene, J. E. *Ab initio* Molecular Dynamics Simulations of Nitrogen/VN (001) Surface Reactions: Vacancy-catalyzed N₂ Dissociative Chemisorption, N Adatom Migration, and N₂ Desorption. *J. Phys. Chem. C* **2016**, *120*, 12503-12516.
- (30) Gudmundsson, M.; Ellingsson, V.; Skúlason, E.; Abghoui, Y. 2021. Optimizing Nitrogen Reduction Reaction on Nitrides: A Computational Study on Crystallographic Orientation. *Top. Catal.*, **2021**, 1-10.
- (31) Cappus, D.; Haßel, M.; Neuhaus, E.; Heber, M.; Rohr, F.; Freund, H. J. Polar Surfaces of Oxides: Reactivity and Reconstruction. *Surf. Sci.* **1995**, *337*, 268-277.
- (32) Dong, B.; Oyelade, A.; Nandagopal, N.; Kelber, J. A. Aromatic-Doped Boron Carbide Films Formed by PECVD of Metacarborane and Aniline or Pyridine: Chemical and Electronic Structure. *Surf. Coat. Technol.* **2017**, *314*, 45-50.

- (33) Seah, M. P. Quantification of AES and XPS, in *Practical Surface Analysis*, second edition, volume 1- Auger and X-ray Photoelectron Spectroscopy", Seah, M. P. and Briggs, D. (eds). pp. 201-255, Wiley and Sons, New York (1990).
- (34) Hirpara, J.; Chandra, R. Investigation of Optical and Anti-corrosive Properties of Reactively Sputtered Vanadium Oxynitride Thin Films. *Mater. Today* **2021**, *44*, 3065-3069.
- (35) Bard, A. J.; Faulkner, L. R., *Electrochemical Methods: Fundamentals and Applications* (2nd ed.) John Wiley & Sons 2001.
- (36) Biesinger, M. C.; Lau, L. W. M.; Gerson, A. R.; Smart, R. S. C. Resolving Surface Chemical States in XPS Analysis of First Row Transition Metals, Oxides and Hydroxides: Sc, Ti, V, Cu and Zn. *Appl. Surf. Sci.* **2010**, *257*, 887-898.
- (37) Hou, J.; Yang, M.; Zhang, J. Recent Advances in Catalysts, Electrolytes and Electrode Engineering for the Nitrogen Reduction Reaction under Ambient Conditions. *Nanoscale* **2020**, *12*, 69-692.
- (38) Darcy, J. W.; Koronkiewicz, B.; Parada, G. A.; Mayer, J. M. A Continuum of Proton-Coupled Electron Transfer Reactivity. *Acc. Chem. Res.* **2018**, *51*, 2391-2399.
- (39) Kang, S.; Wang, J.; Zhang, S.; Zhao, C.; Wang, G.; Cai, W.; Zhang, H. Plasma-etching Enhanced Titanium Oxynitride Active Phase with High Oxygen Content for Ambient Electrosynthesis of Ammonia. *Electrochem. Commun.* **2019**, *100*, 90-95.
- (40) Moltved, K. A.; Kepp, K. P. The Chemical Bond between Transition Metals and Oxygen: Electronegativity, d-Orbital Effects, and Oxophilicity as Descriptors of Metal–Oxygen Interactions. *J. Phys. Chem. C* **2019**, *123*, 18432-18444.

- (41) Du, H.; Gengenbach, T. R.; Hodgetts, R.; MacFarlane, D. R.; Simonov, A. N. Critical Assessment of the Electrocatalytic Activity of Vanadium and Niobium Nitrides toward Dinitrogen Reduction to Ammonia. *ACS Sustainable Chem. Eng.* **2019**, *7*, 6839-6850.
- (42) Huang, L.; Wu, J.; Han, P.; Al-Enizi, A. M.; Almutairi, T. M.; Zhang, L.; Zheng, G. NbO₂ Electrocatalyst Toward 32% Faradaic Efficiency for N₂ Fixation. *Small methods* **2019**, *3*, 1800386

Table of contents

